SCIENTIFIC REPORTS

OPEN

SUBJECT AREAS:
GENE REGULATION
CELL SIGNALLING
TRANSLATION
POST-TRANSLATIONAL MODIFICATIONS

Received
11 January 2012

Accepted
14 May 2012

Published
28 May 2012

Correspondence and requests for materials should be addressed to J.A. (admin.auwerx@epfl.ch)

* These authors contributed equally to this work.

Muscle or liver-specific Sirt3 deficiency induces hyperacetylation of mitochondrial proteins without affecting global metabolic homeostasis

Pablo J. Fernandez-Marcos[1,2]*, Ellen H. Jeninga[1]*, Carles Canto[1,3], Taoufiq Harach[1], Vincent C. J. de Boer[4], Penelope Andreux[1], Norman Moullan[1], Eija Pirinen[1,5], Hiroyasu Yamamoto[1], Sander M. Houten[4], Kristina Schoonjans[1] & Johan Auwerx[1]

[1]Laboratory of Integrative and Systems Physiology (LISP/NCEM), School of Life Sciences, Ecole Polytechnique Fédérale de Lausanne (EPFL), 1015 Lausanne, Switzerland, [2]Laboratory of Tumor Suppression, Molecular Oncology Program, Spanish National Cancer Research Center (CNIO), Madrid, 28090, Spain, [3]Nestlé Institute of Health Sciences, 1015, Lausanne, Switzerland, [4]Laboratory of Genetic Metabolic Diseases, Academic Medical Center, Meibergdreef 9, 1105 AZ, Amsterdam, The Netherlands, [5]Biotechnology and Molecular Medicine, A.I. Virtanen Institute for Molecular Sciences, Biocenter Kuopio, University of Eastern Finland, Kuopio, Finland.

***Sirt3* is a mitochondrial sirtuin, predominantly expressed in highly metabolic tissues. Germline ablation of *Sirt3* has major metabolic consequences, including increased susceptibility to metabolic damage and oxidative stress after high fat feeding. In order to determine the contribution of liver and skeletal muscle to these phenotypes, we generated muscle-specific *Sirt3* ($Sirt3^{skm-/-}$) and liver-specific *Sirt3* ($Sirt3^{hep-/-}$) knock-out mice. Despite a marked global hyperacetylation of mitochondrial proteins, $Sirt3^{skm-/-}$ and $Sirt3^{hep-/-}$ mice did not manifest any overt metabolic phenotype under either chow or high fat diet conditions. Similarly, there was no evidence for increased oxidative stress in muscle or liver when *Sirt3* was ablated in a tissue-specific manner. These observations suggest that the mitochondrial hyperacetylation induced by *Sirt3*-deletion in a tissue specific manner is not necessarily linked to mitochondrial dysfunction and does not recapitulate the metabolic abnormalities observed in the germline *Sirt3* knock-out mice.**

Sirt3 is one of the 7 members of the sirtuin family of NAD^+-dependent deacetylases. Together with Sirt4 and Sirt5, Sirt3 localizes predominantly in the mitochondria[1]. Importantly, Sirt3 is a primary regulator of mitochondrial protein acetylation. The absence of *Sirt3* enhances global acetylation of mitochondrial proteins, while no significant changes in protein acetylation were observed in $Sirt4^{-/-}$ and $Sirt5^{-/-}$ mitochondria[2]. *Sirt3* expression is highly enriched in metabolic tissues like liver, brown adipose tissue (BAT), heart, skeletal muscle and kidney[3]. *Sirt3* expression increases in muscle after exercise training, fasting and caloric restriction (CR), while it decreases upon long-term high fat feeding[4,5]. In liver and BAT *Sirt3* expression also increases after CR and fasting, as well as upon cold exposure in BAT[3,6].

Germline $Sirt3^{-/-}$ mice display increased levels of cellular reactive oxygen species (ROS)[7–12] and impaired cellular respiration after prolonged fasting[6] in different tissues, including the muscle, liver, brain or the inner ear. In contrast, *Sirt3* overexpression *in vitro* enhances mitochondrial respiration[13] and reduces ROS production[3]. Not surprisingly, whole body *Sirt3* knock-out mice are sensitized to high fat diet (HFD)-induced obesity, insulin resistance, hyperlipidemia and steatohepatitis[14]. The etiology of such defects might be found in the ability of Sirt3 to enhance fat oxidation and improve anti-oxidant defences[6,9,10,14–16]. However, while recent reports show that Sirt3 suppresses oxidative stress under CR[9,10,12], it still remains to be elucidated whether Sirt3 might influence HFD-induced oxidative stress.

All studies to date used germline *Sirt3* deficient mice to study the role of Sirt3 on metabolism, making it impossible to distinguish the contribution of individual tissues to the phenotypic changes. Liver and muscle are two of the most important tissues determining whole body metabolism: skeletal muscle is the largest organ in mammals, contributing to ±40% of the body mass, and it plays a major role in whole body metabolism, as it is vital for insulin-mediated glucose disposal and lipid catabolism. In turn, the liver is central to regulate glucose, lipid and cholesterol homeostasis. Altered function of these tissues is, thus, likely to contribute to the systemic

metabolic disturbances observed in the germline *Sirt3* knock-out mice. Here, we report the generation of the first set of tissue-specific *Sirt3* knockout mouse models in muscle and liver, and describe how *Sirt3* deletion in these tissues, despite leading to mitochondrial protein hyperacetylation, has minor phenotypic consequences. This suggests that the metabolic abnormalities observed in the germline *Sirt3*-KO mice may not stem from the liver or muscle deficiencies.

Results

Generation of the Sirt3$^{skm-/-}$ and Sirt3$^{hep-/-}$ mice. To investigate the role of Sirt3 in muscle and liver, as well as its impact on whole body metabolism, we generated a mouse line in which exons 2 and 3 were flanked with LoxP sites, priming it for subsequent deletion using the Cre-LoxP system (Fig. 1A). *Sirt3*$^{L2/L2}$ mice, bearing floxed *Sirt3* L2 alleles, were bred with mice expressing the Cre recombinase under the control of the human α-skeletal actin promoter[17], yielding HSA-Cre$^{Tg/0}$/*Sirt3*$^{L2/L2}$ mutants (*Sirt3*$^{skm-/-}$), in which *Sirt3* is selectively ablated in the skeletal muscles. A distinct mouse line, in which Cre expression was under the control of the albumin promoter[18], was used to generate Alb-Cre$^{Tg/0}$/*Sirt3*$^{L2/L2}$ mice (*Sirt3*$^{hep-/-}$), in which *Sirt3* is selectively ablated in the liver.

Sirt3$^{skm-/-}$ and *Sirt3*$^{hep-/-}$ mice were born at a normal Mendelian ratio and had a normal appearance. Only residual *Sirt3* mRNA levels were detected in skeletal muscle (gastrocnemius, soleus and EDL) of 8-week-old *Sirt3*$^{skm-/-}$ mice (Fig. 1B), demonstrating that *Sirt3* was efficiently ablated in *Sirt3*$^{skm-/-}$ muscles. In addition to the skeletal muscle, a 35% reduction in *Sirt3* mRNA levels was observed in the heart of *Sirt3*$^{skm-/-}$ mice, whereas no significant reduction was seen in other tissues (Fig. 1B). *Sirt3* mRNA levels were also blunted in livers from *Sirt3*$^{hep-/-}$ mice of 8 weeks of age, but normal in other tissues (Fig. 1C). In line with the above results, the Sirt3 protein was undetectable in the skeletal muscle of *Sirt3*$^{skm-/-}$ mice, but remained unaffected in the liver (Fig. 1D); conversely the Sirt3 protein was only absent in the liver in the *Sirt3*$^{hep-/-}$ mice (Fig. 1E), confirming that the *Sirt3* deletion is efficient and restricted to the targeted tissue.

The absence of *Sirt3* had no impact on the expression of a vast set of metabolic genes in either muscle (Fig. 1F) or liver (Fig. 1G). Of note, we did not detect any compensatory increase in the expression of the other mitochondrial sirtuins (*Sirt4* and *Sirt5*) in the two *Sirt3*-deficient tissues. We also determined *Pgc1α* and *Scd1* expression, two genes whose levels were reported to be altered in germline *Sirt3*-KO tissues[5,14]; however, we could not detect any significant change in their expression in our mutant mice. These results suggest that

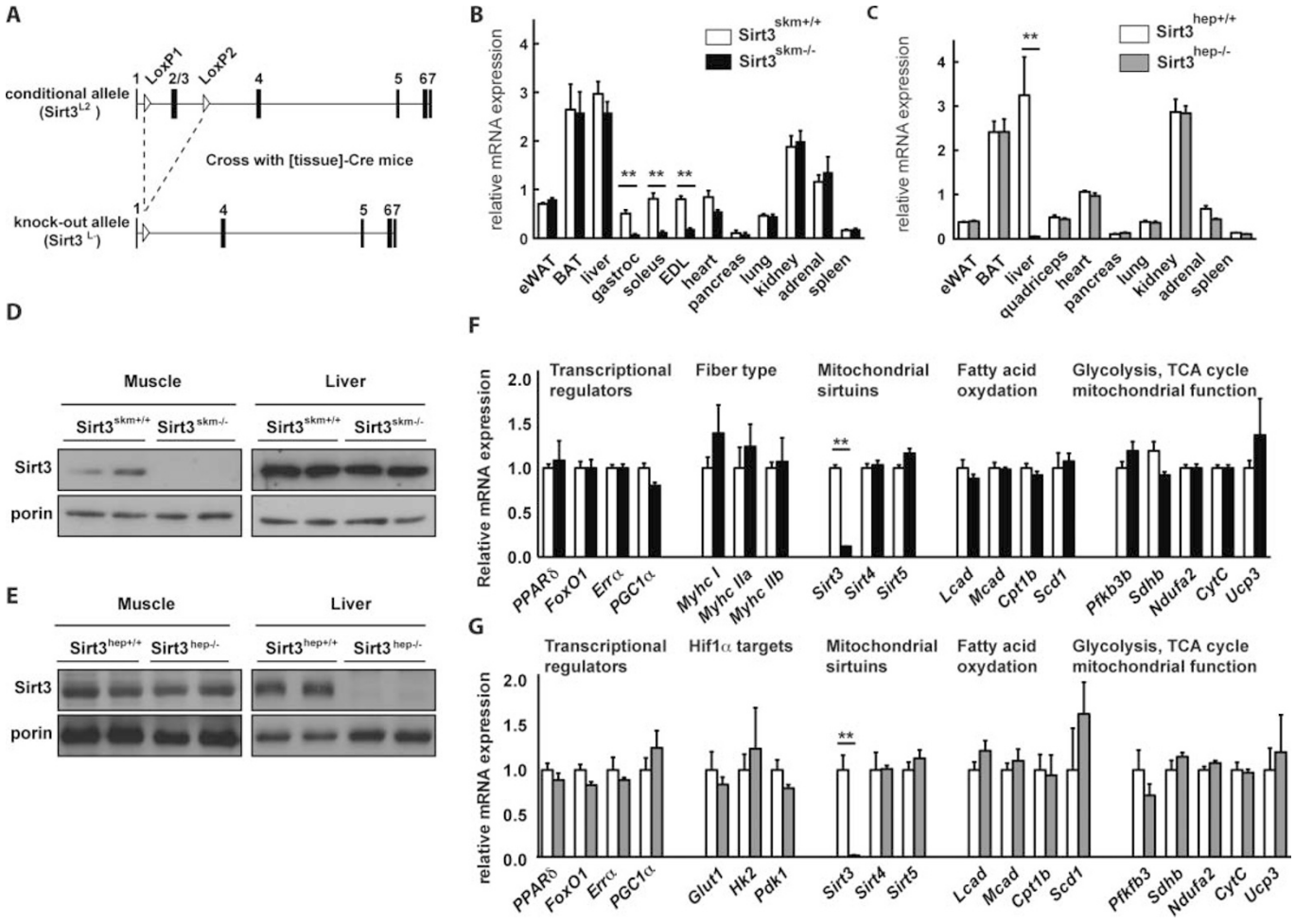

Figure 1 | Generation, validation and expression of metabolic genes for the *Sirt3*$^{hep-/-}$ and *Sirt3*$^{skm-/-}$ mice. (A) Targeting strategy used to generate the tissue-specific *Sirt3*-deficient mice. Maps of the *Sirt3* genomic locus showing the conditional allele (upper panel) and the KO allele (lower panel). The white arrowheads indicate the LoxP sites and the black vertical bars represent the respective exons. (B–C) Sirt3 mRNA expression levels in different tissues of *Sirt3*$^{skm+/+}$ and *Sirt3*$^{skm-/-}$ mice (B) and of *Sirt3*$^{hep+/+}$ and *Sirt3*$^{hep-/-}$ mice (C); n=4 per group. (D–E) Sirt3 protein expression as assessed by western blotting in muscle (D) and liver (E) of the *Sirt3*-deficient mouse models. Porin is used as a loading control. (F–G) Gene expression in gastrocnemius muscle of *Sirt3*$^{skm+/+}$ and *Sirt3*$^{skm-/-}$ mice (F) and in liver of *Sirt3*$^{hep+/+}$ and *Sirt3*$^{hep-/-}$ mice (G) after 18 weeks of HFD. mRNA levels were normalized to 36B4. Data represent the mean ± SEM for at least four animals per group.

muscle or liver-specific deletion of *Sirt3* does not have a major impact on the expression of genes involved in metabolic control. We only performed this gene expression analysis in mice subjected to HFD, since young, unchallenged mice show no phenotype whatsoever, both in our hands and in previous reports[2].

Normal metabolic phenotype in Sirt3$^{hep-/-}$ mice fed chow or high fat diet. We next subjected *Sirt3*$^{hep+/+}$ and *Sirt3*$^{hep-/-}$ mice to a standardized phenotyping protocol before and after high fat diet (HFD) feeding (Fig. 2A). Body weight and body composition were similar in both genotypes before and after HFD (Fig. 2B and 2C). The weight gain curves of the *Sirt3*$^{hep-/-}$ mice were indistinguishable from those of the *Sirt3*$^{hep+/+}$ mice (data not shown). During indirect calorimetry using the comprehensive lab animal monitoring system (CLAMS), no difference was observed in food intake (Fig. 2D), mean VO_2 (Fig. 2E), mean respiratory exchange ratio (RER) (Fig. 2F) or spontaneous locomotor activity (Fig. 2G), before and after HFD. At sacrifice, the weight of the liver, epididymal white fat or interscapular brown fat depots were not different between the genotypes (Fig. 2H). To specifically test the contribution of *Sirt3* deletion in the liver to glucose homeostasis we performed an intraperitoneal glucose tolerance test (ipGTT) and an insulin tolerance test (ipITT) both before (data not shown) and after HFD. Again no significant differences between *Sirt3*$^{hep+/+}$ and *Sirt3*$^{hep-/-}$ animals were detected in these experiments (Fig. 2I, 2J and data not shown). All these data contrast with the results obtained in germline *Sirt3*-deficient mice, where *Sirt3*-deficiency was shown to sensitize the liver to HFD-induced damage[14].

Germline *Sirt3*-KO mice have also been reported to display altered aminoacid profiles in blood and liver[15]. We therefore also analyzed the blood aminoacid profiles, but could not detect differences between the *Sirt3*$^{hep-/-}$ and *Sirt3*$^{hep+/+}$ samples, both in the fed state (data not shown) and after a 24 h fast (Fig. 2K).

Sirt3 has also been suggested to act as a key modulator of ketone body production, a glucose-sparing energy substrate in the fasting state mostly synthesized by hepatocytes[19]. However, blood levels of β-hydroxybutyrate, a surrogate marker of the activity of this pathway, were similar in *Sirt3*$^{hep+/+}$ and *Sirt3*$^{hep-/-}$ mice both before and after a 24 h fast at 8-weeks of age (Fig. 2L). This contrasts with the germline *Sirt3* knock-out mice, which displayed a maximal decrease in β-hydroxybutyrate after a 24 h fast[19].

Finally, since germline *Sirt3*-KO mice display abnormal fatty acid metabolism and aberrant blood acylcarnitine profiles[14,15], we analyzed the blood acylcarnitines in *Sirt3*$^{hep+/+}$ and *Sirt3*$^{hep-/-}$ animals in both fed (data not shown) and fasted (24 h fast) states

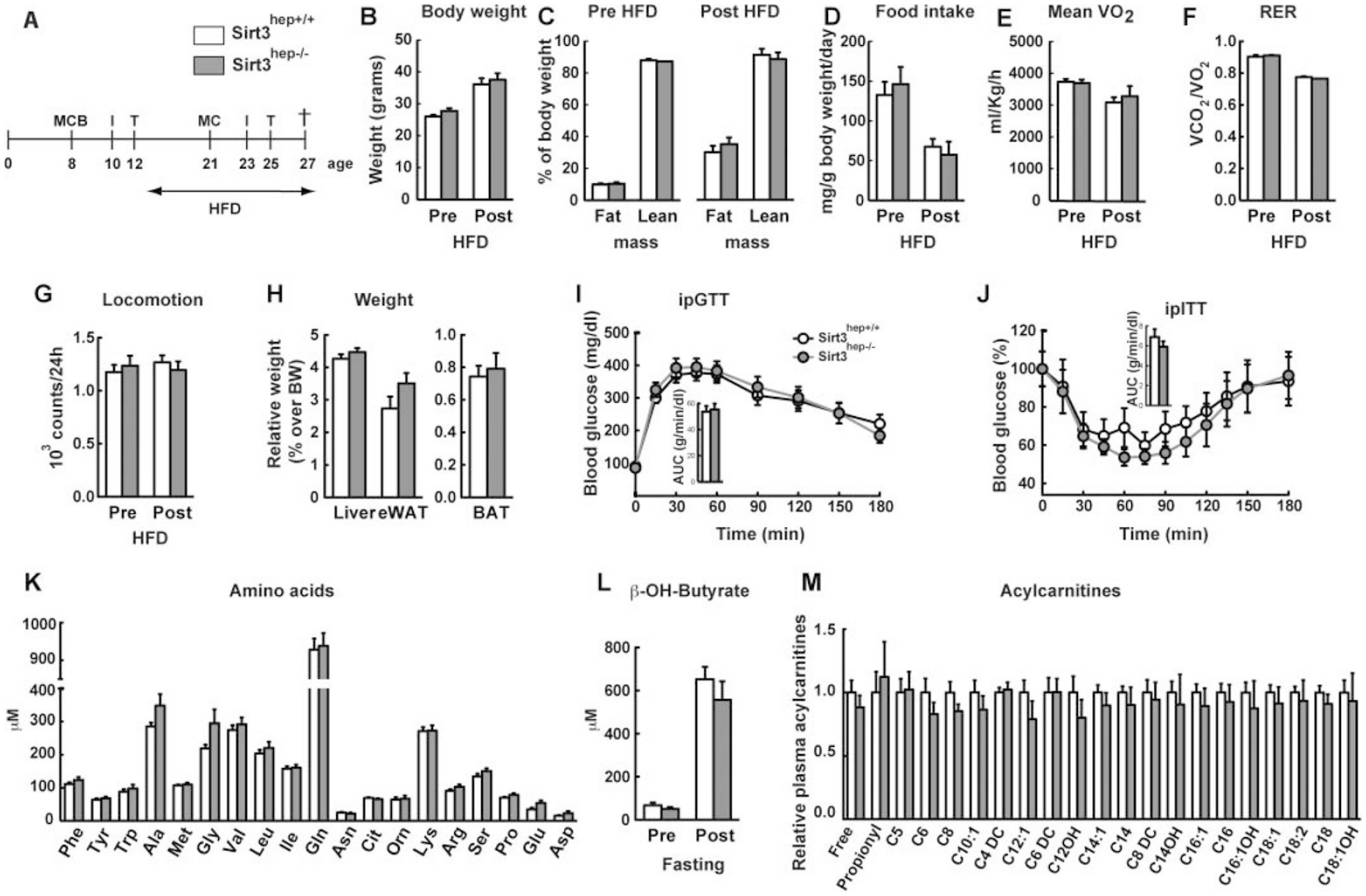

Figure 2 | Metabolic phenotyping of *Sirt3*$^{hep-/-}$ mice. (A) Experimental schedule of the clinical phenotyping protocol. MCB: non-invasive monitoring of body fat and lean mass by EchoMRI, energy expenditure by indirect calorimetry (CLAMS system), and blood sampling for metabolite analysis; I: intra-peritoneal glucose tolerance test (ipGTT); T: intra-peritoneal insulin tolerance test (ipITT); †: sacrifice and collection of blood and organs for further analysis. (B) Body weight and (C) body composition of *Sirt3*$^{hep+/+}$ and *Sirt3*$^{hep-/-}$ mice before and after 8 weeks of HFD. (D–G) Daily food intake (D), mean O_2 consumption (VO_2; E), mean respiratory exchange ratio (RER; F) and total ambulatory locomotor activity (G) as measured over a 24 h period before and after HFD. (H) Relative weight of tissues normalized by body weight in *Sirt3*$^{hep+/+}$ and *Sirt3*$^{hep-/-}$ mice. (I–J) Intra-peritoneal glucose tolerance test (ipGTT; I), and intra-peritoneal insulin tolerance test (ipITT; J) in mice fed a HFD for 15-17 weeks. The bar graphs represent the average area under the curve (AUC). (K) Levels of the indicated aminoacids were determined in plasma from 8 weeks old male mice. (L) β-hydroxy-butyrate was analysed in plasma from 8 weeks old male mice before and after a 24h fasting period. (M) Acylcarnitine levels in plasma from 8 weeks old male mice. Results are represented as mean values (n=8−10 mice for each group) ± standard error of the mean (SEM).

(Fig. 2M), but again could not detect any significant difference in the acylcarnitine levels between the two genotypes.

All these findings combined suggest that the altered metabolic response of germline *Sirt3*-KO mice subjected to HFD[14] or to fasting[15,19] are not due to the absence of *Sirt3* in hepatocytes, but rather stem from the indirect effect of *Sirt3* ablation in some other tissue.

No metabolic phenotype in Sirt3$^{skm-/-}$ mice under chow or high fat diet. We next determined whether the phenotype observed in the germline *Sirt3* knock-out mice could be due to another major metabolic tissue, i.e. the skeletal muscle. We therefore subjected *Sirt3*$^{skm-/-}$ and *Sirt3*$^{skm+/+}$ mice to a similar phenotyping protocol than the one described for the liver-specific *Sirt3*-deficient mice (Fig. 3A). No differences in body weight (Fig. 3B) and body composition (Fig. 3C) were observed between *Sirt3*$^{skm-/-}$ and *Sirt3*$^{skm+/+}$ mice, even under HFD conditions. Consistent with the similarities in body weight, evaluation using CLAMS indicated that food intake (Fig. 3D), mean VO_2 (Fig. 3E), mean RER (Fig. 3F) and spontaneous locomotor activity (Fig. 3G) were similar between the two genotypes before and after HFD. In addition, no significant differences were observed in the weight of different tissues at sacrifice (Fig. 3H). Upon an intraperitoneal glucose tolerance test (ipGTT) the glucose excursion (Fig. 3I; left panel) and glucose-induced insulin secretion (Fig. 3I; right panel) were comparable between the two genotypes. Also, the drop and recovery of blood glucose levels upon an intraperitoneal insulin tolerance test (ipITT) were, again, not distinct between the two genotypes (Fig. 3J).

To further evaluate possible phenotypic differences between the *Sirt3*$^{skm-/-}$ and *Sirt3*$^{skm+/+}$ mice, we exposed the mice to a cold challenge (4°C). Mice from both genotypes similarly maintained their core body temperature for at least 6 hours after a 24 h fast (Fig. 3K), or after 14 weeks of HFD (Supl. Fig. 1A), indicating that muscle *Sirt3* is not essential for cold-induced adaptive thermogenesis. Exercise increases *Sirt3* expression in muscle[4,5], suggesting a role for *Sirt3* in exercise physiology. *Sirt3*$^{skm-/-}$ and *Sirt3*$^{skm+/+}$ mice, however, ran a similar distance until exhaustion both before and after HFD (Fig. 3L). Also no difference in endurance running was present before and after a 24 h fast (Supp. Fig. 1B). In addition, both the heart rate (Fig. 3M) and systolic blood pressure (Fig. 3N) were similar between *Sirt3*$^{skm-/-}$ and *Sirt3*$^{skm+/+}$ mice, indicating that the partial reduction in *Sirt3* mRNA levels found in the *Sirt3*$^{skm-/-}$ hearts has no major impact on cardiac function.

Altogether, these data indicate that *Sirt3*$^{skm-/-}$ mice are metabolically indistinguishable from control mice under both chow and HFD. Thus, the absence of *Sirt3* in the skeletal muscle by itself cannot

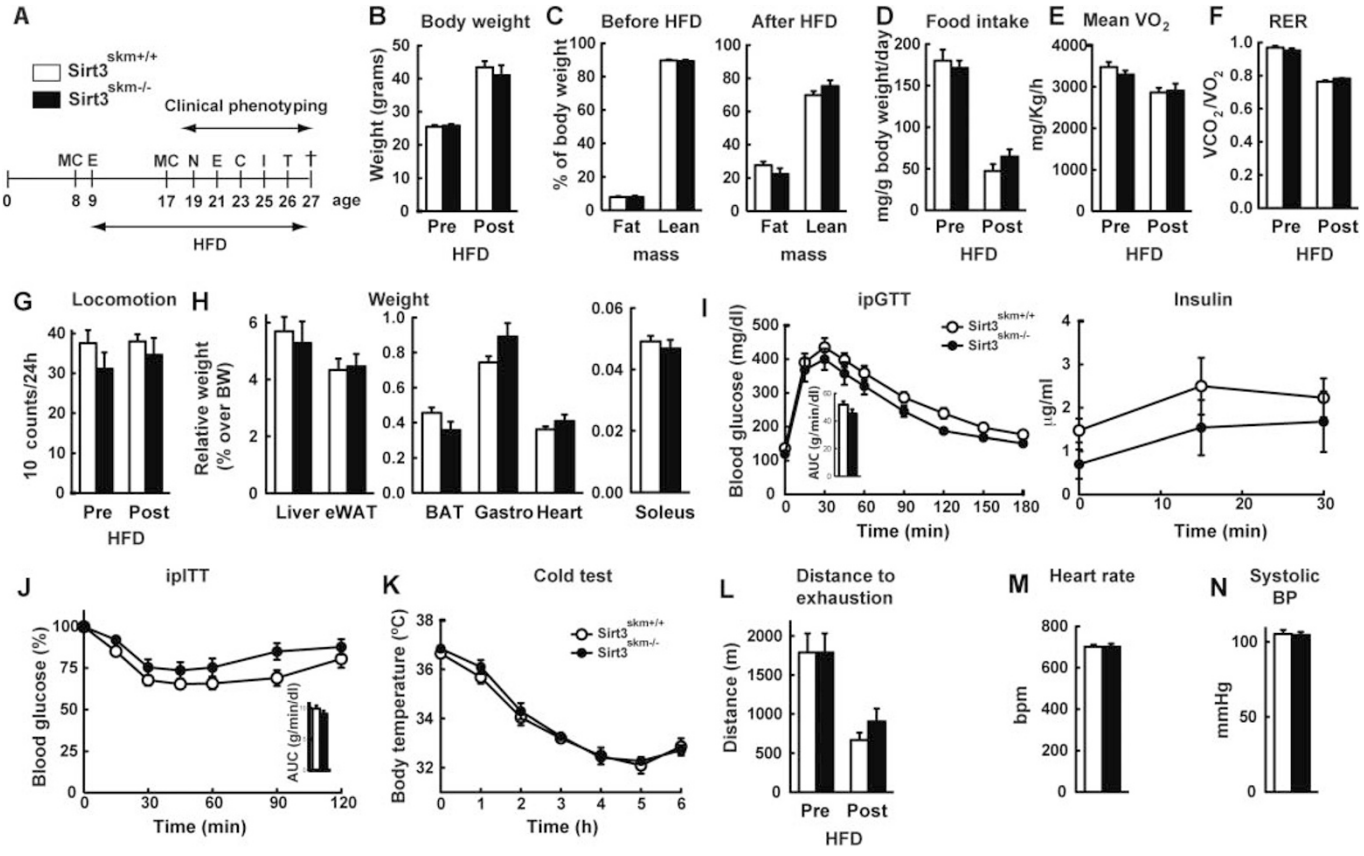

Figure 3 | Metabolic phenotyping of *Sirt3*$^{skm-/-}$ mice. (A) Experimental schedule of the clinical phenotyping protocol. For abbreviations see legend of Fig. 2A; E: endurance exercise on a treadmill; N: non-invasive blood pressure measurement (NIBP); C: cold test. (B) Body weight and (C) body composition of *Sirt3*$^{skm+/+}$ and *Sirt3*$^{skm-/-}$ mice before and after 8 weeks of HFD. (D–G) Daily food intake (D), mean O_2 consumption (VO_2; E), mean respiratory exchange ratio (RER; F) and total ambulatory locomotor activity (G) as measured over a 24 h period before and after HFD. (H) Relative weight of tissues normalized by body weight in *Sirt3*$^{skm+/+}$ and *Sirt3*$^{skm-/-}$ mice. (I) Intra-peritoneal glucose tolerance test (ipGTT, left panel) and plasma insulin during ipGTT (right panel) in mice fed a HFD for 16 weeks. (J) Intra-peritoneal insulin tolerance test (ipITT) in *Sirt3*$^{skm+/+}$ and *Sirt3*$^{skm-/-}$ mice fed a HFD for 17 weeks. (I and J) The bar graph (inner panels) represents the average area under the curve (AUC). (K) *Sirt3*$^{skm+/+}$ and *Sirt3*$^{skm-/-}$ mice fasted for 24h were exposed to 4°C for 6 h and rectal temperature was monitored. (L) Endurance exercise test on *Sirt3*$^{skm+/+}$ and *Sirt3*$^{skm-/-}$ mice before and after 12 weeks of HFD. (M) Heart rate and (N) systolic blood pressure were measured in *Sirt3*$^{skm+/+}$ and *Sirt3*$^{skm-/-}$ mice after 10 weeks on HFD. Results are presented as mean values (n=8−10 mice for each group) ± SEM.

explain the metabolic phenotype observed in the germline deficient *Sirt3*-KO animals.

Mitochondrial protein hyperacetylation but normal oxidative stress in Sirt3-deficient tissues. The fact that Sirt3 is a mitochondrial protein prompted us to investigate the integrity of the mitochondria in both tissue-specific $Sirt3^{-/-}$ mouse models after HFD treatment, a stress after which we expect the effects of *Sirt3* deficiency to be accentuated. The protein levels of subunits from the mitochondrial respiratory complexes I, II, IV and V were indistinguishable in $Sirt3^{skm-/-}$ and $Sirt3^{skm+/+}$ muscle, and in $Sirt3^{hep-/-}$ and $Sirt3^{hep+/+}$ liver (Fig. 4A). In line with the observations in germline $Sirt3^{-/-}$ mice[2], there was a marked increase in global mitochondrial protein acetylation in the tissues where the *Sirt3* gene had been deleted (Fig. 4B and 4C). We next evaluated the acetylation levels of specific Sirt3 targets. Sirt3 interacts with and deacetylates Ndufa9, a subunit of complex I[13]. Consistently, we observed increased acetylation of some members of the Ndufa9-containing complex I in livers from the $Sirt3^{hep-/-}$ mice or quadriceps muscle from the $Sirt3^{skm-/-}$ mice, as compared with their respective wild type controls (Fig. 4D, top panels). However, this increased acetylation did not lead to any change in maximal complex I or complex IV activities (Fig. 4E). As an internal control, we measured the activity of citrate synthase, a mitochondrial enzyme from the Krebs cycle not belonging to the electron transport chain, whose activity was also unchanged in the absence of Sirt3 in both mouse models (Fig. 4E). To further examine mitochondrial function in the absence of *Sirt3* we measured oxygen consumption in $Sirt3^{L2/L2}$ primary hepatocytes-with the *Sirt3* gene flanked with LoxP sites- in which we acutely deleted the *Sirt3* gene by an adenoviral infection with Cre. Oxygen consumption rate (OCR) was not affected by the absence of *Sirt3* (Fig. 4F and Suppl. Fig. 2A).

Sirt3 deficiency has also been correlated with low levels of cellular ATP[13]. We therefore measured ATP levels in $Sirt3^{skm+/+}$ and $Sirt3^{skm-/-}$ gastrocnemius muscle and in $Sirt3^{hep+/+}$ and $Sirt3^{hep-/-}$ liver, but could not detect differences between tissues from the different genotypes

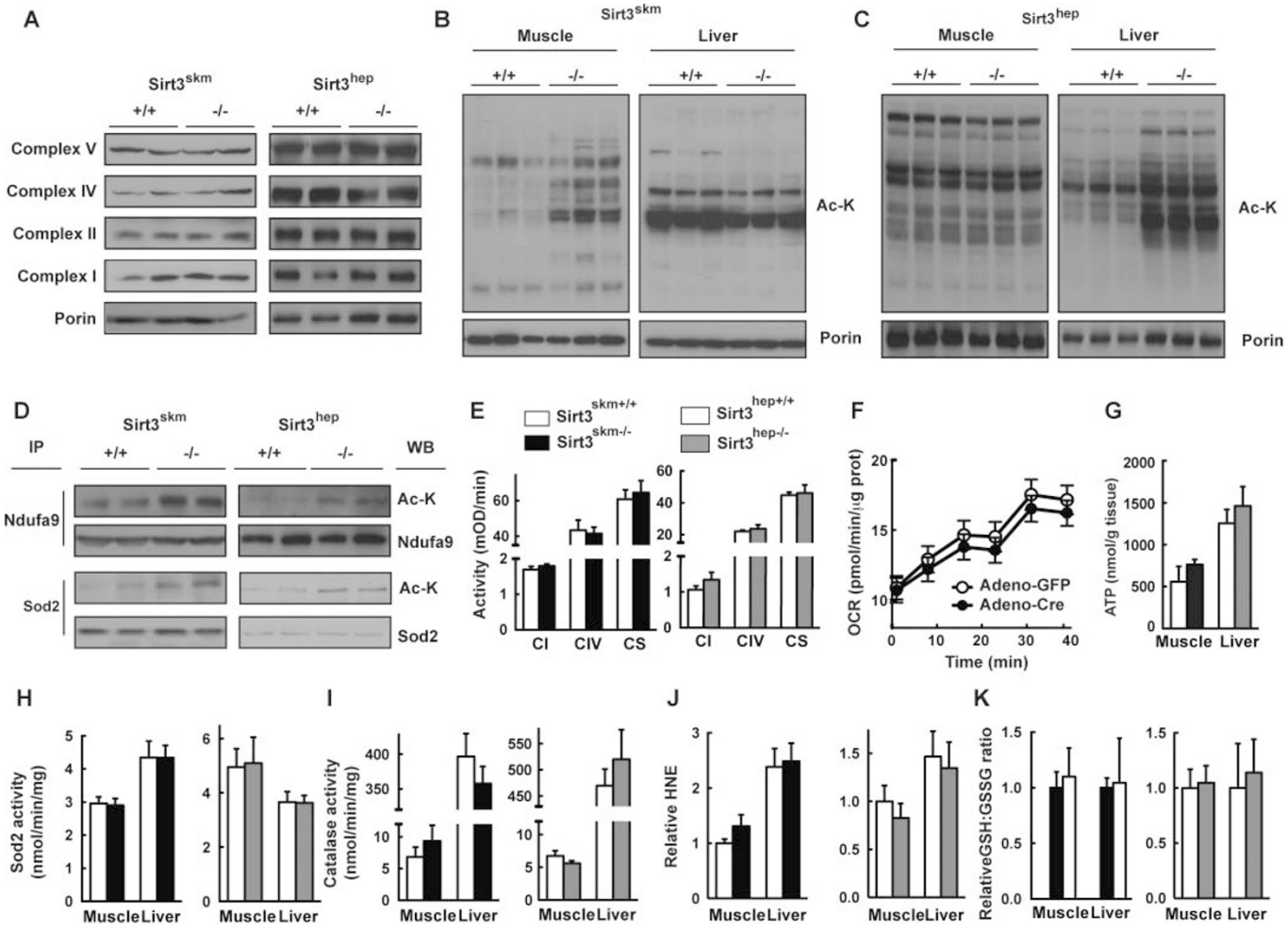

Figure 4 | Hyperacetylation of mitochondrial proteins but normal ROS markers in $Sirt3^{hep-/-}$ and $Sirt3^{skm-/-}$ mice subjected to HFD. (A) Protein expression levels of complex I, II, IV and V in isolated mitochondria of $Sirt3^{skm+/+}$ and $Sirt3^{skm-/-}$ muscle (left panels) and $Sirt3^{hep+/+}$ and $Sirt3^{hep-/-}$ livers (right panels). (B, C) Acetylation status of mitochondrial proteins extracted from muscle and liver of $Sirt3^{skm+/+}$ and $Sirt3^{skm-/-}$ mice (B) and $Sirt3^{hep+/+}$ and $Sirt3^{hep-/-}$ mice (C). Mitochondrial protein lysates were subjected to western blotting using an anti-acetylated lysine antibody (Ac-K) and porin as a loading control. (D) Acetylation level of complex I members (top two rows of panels) and Sod2 (bottom two rows of panels) in $Sirt3^{skm+/+}$ and $Sirt3^{skm-/-}$ muscle (left panels) or $Sirt3^{hep+/+}$ and $Sirt3^{hep-/-}$ livers (right panels). Endogenous Ndufa9 or Sod2 were immunopurified from muscle lysates and immunoblotted using Ndufa9/Sod2 and Ac-K antibodies. (E) Complex I (CI), complex IV (CIV) and Citrate synthase (CS) activities in $Sirt3^{skm+/+}$ and $Sirt3^{skm-/-}$ muscle (left panel) or $Sirt3^{hep+/+}$ and $Sirt3^{hep-/-}$ (right panel). (F) Oxygen consumption rate (OCR) from primary hepatocytes obtained from $Sirt3^{L2/L2}$ mice infected with the indicated viruses. (G) ATP levels were measured from the indicated tissue lysates. (H–K) Activities of mitochondrial Sod2 (H) and catalase (I) and levels of 4-hydroxy-2-nonenal (HNE; J) and GSH/GSSG ratio (K) in muscle and liver lysates of $Sirt3^{skm+/+}$ and $Sirt3^{skm-/-}$ mice (left panels) or $Sirt3^{hep+/+}$ and $Sirt3^{hep-/-}$ mice (right panels). Measurements in panels E–K were determined using samples from at least four mice per genotype. All the samples used for these studies come from mice subjected to the HFD treatment, sacrificed in fed state. Data are represented as mean ± SEM.

(Fig. 4G). Accordingly, we did not detect differences in the phosphorylation status of the AMP/ATP sensing AMP-activated protein kinase (AMPK), suggesting that *Sirt3* deletion in a tissue-specific fashion does not affect intracellular energy charge (Suppl. Fig. 2B).

Sirt3 has been shown to reduce oxidative stress, mostly through deacetylating and activating the mitochondrial ROS scavenger Sod2[9,10,12,16]. We therefore also determined Sod2 acetylation status in the absence of *Sirt3*; as reported, *Sirt3*-deficient tissues presented increased levels of acetylated Sod2 (Fig. 4D, lower panels). In contrast, *Sirt3* gene ablation did not affect the activity of Sod2 (Fig. 4H), nor that of catalase, another key ROS scavenger (Fig. 4I). We next measured a few markers of oxidative stress, such as the level of 4-hydroxy-2-nonenal (HNE; a marker for lipid peroxidation) and glutathione, in liver and muscle from our mutant mouse models after HFD treatment. No difference in these parameters was observed between *Sirt3*-deficient tissues and their respective controls (Fig. 4J-K). These results show that tissue-specific ablation of *Sirt3* results in increased acetylation of ROS scavengers, but that this alteration is not sufficient to affect their activity, which may help to explain the lack of a metabolic phenotype in these two tissue-specific *Sirt3* deficient mouse models.

Discussion

We report here the generation and phenotypic characterization of the first set of tissue-specific *Sirt3* knockout mice (muscle-specific $Sirt3^{skm-/-}$ and liver-specific $Sirt3^{hep-/-}$ mice). Consistent with the role of Sirt3 as the major mitochondrial deacetylase[2], mitochondrial proteins were robustly hyperacetylated in *Sirt3*-deficient tissues. In line with this observation, specific Sirt3 targets, such as mitochondrial complex I and the mitochondrial ROS scavenger, Sod2, were also markedly hyperacetylated in *Sirt3*-deficient tissues (Fig. 4D), as previously described in livers from the germline $Sirt3^{-/-}$ mice[9,12,13]. However, the activities of these enzymes (Fig. 4H–I) were not changed in *Sirt3*-deficient tissues, which indicates that hyperacetylation of these proteins does not necessarily result in a change in their maximal activity. Indeed, while many residues might be acetylated in a single protein, only the acetylation of a few key residues crucially determines the enzymatic activity/function of the protein, as demonstrated with LCAD[6]. This phenomenon might explain the lack of a metabolic phenotype in the tissue-specific *Sirt3*-deficient mice.

Several *in vivo* and *in vitro* studies demonstrated a role for Sirt3 in the suppression of oxidative stress[3,8–12,16]. However, different groups have reported normal ROS levels in basal state in liver, brain or cochlea[9,10]. In line with these last reports, we observed normal levels of surrogate markers for ROS in *Sirt3*-deficient tissues, as well as similar levels of activity of the mitochondrial ROS scavengers Sod2 and catalase (Fig. 4 H–I). Again, these results might explain the lack of a clear metabolic phenotype in the conditions we tested.

Despite the higher mitochondrial protein hyperacetylation, the tissue-specific $Sirt3^{-/-}$ mice described here were metabolically similar to control littermates in all the conditions that we tested (chow and HFD diet, 24 h fasting, exercise or cold). Our results therefore imply that the previously described phenotypes of germline $Sirt3^{-/-}$ animals under a short fasting or HFD[6,9–11,13–15,19] are not due to the absence of *Sirt3* specifically in liver or muscle. Rather, our data indicate that either *Sirt3* deficiency in another tissue or the coordinated defect of *Sirt3* in multiple tissues accounts for these effects in the germline *Sirt3* knock-out mice. In this regard, our results do also not rule out the possibility that latent defects in muscle or liver function in our models can be fully compensated by another tissue or sirtuin function. In this sense, further tissue-specific *Sirt3* deficient mouse models exploring the brain, white or brown adipose, or macrophage function of *Sirt3* will be key to fully evaluate the etiology of the metabolic alterations in the germline *Sirt3* knock-out mice. In this context it is interesting to note that no change in *Sirt3* mRNA or protein expression in non-targeted tissues (Fig. 1B, 1C, 1D and 1E), nor any change in the mRNA levels of the other mitochondrial sirtuins (*Sirt4* and *Sirt5*) in the *Sirt3*-targeted tissues (Fig. 1F and 1G) was present, which suggest that there is no compensation by other mitochondrial sirtuins. These observations, however, do not rule out a change in the activity, rather than in mRNA or protein levels, of these sirtuins as the possible mechanism of compensation.

Of note is also that $Sirt3^{skm-/-}$ mice, when subjected to a 24 h fast and, subsequently, to a cold test, do not suffer hypothermia, as previously reported for the whole-body *Sirt3*-KO mice[6]. Since the two main tissues responsible for temperature homeostasis are muscle and brown fat, and *Sirt3* is highly expressed in this last tissue, it is tempting to speculate that *Sirt3* in brown fat, but not in skeletal muscle, plays an important role in temperature homeostasis, most probably via regulation of mitochondrial uncoupling. Brown fat is also an important tissue in fat and glucose clearance, and increased brown fat amounts or activity can significantly improve global metabolism[20,21]. Thus, one possibility is that the brown fat tissue in $Sirt3^{hep-/-}$ and $Sirt3^{skm-/-}$ mice could compensate for the tissue-specific ablation of *Sirt3* in liver or muscle.

Finally, when comparing studies from different laboratories, it is important to bear in mind that the genetic background and/or the exact composition of the diets are key determinants of phenotypic outcome, which is the result of gene-environment interactions[22,23]. In this regard, our mice were on an obesity-prone background (C57BL/6)[23–25] and fed with a standard HFD, with 60% calories coming from fat, both conditions being different from those used in other reports[14]. Furthermore, differences in the developmental onset of the *Sirt3* gene deletions need to be considered, as germline *Sirt3*-KO mouse model lacks *Sirt3* from the beginning of embryonic development, while the tissue-specific promoters used in our work are activated only from a certain developmental stage.

In summary, our work confirms the critical impact of *Sirt3* on global mitochondrial acetylation. It is unclear why these alterations do not have a major physiological impact when occurring in a tissue-specific manner in muscle or liver, as in our study. Further investigations to understand this conundrum are therefore warranted.

Methods

Generation and clinical phenotyping of the $Sirt3^{hep-/-}$ and $Sirt3^{skm-/-}$ mice. *Sirt3* floxed ($Sirt3^{L2/L2}$) mice were generated using standard gene targeting procedures[26]. These animals were crossed with liver-specific Cre-expressing mice (Alb-Cre)[18] to obtain the $Sirt3^{hep-/-}$ mouse line; or with the skeletal muscle-specific Cre-expressing line (HSA-Cre)[17] to obtain the $Sirt3^{skm-/-}$ line. These two mouse lines were backcrossed onto a pure C57BL/6J background. All animal work in the manuscript has been performed according to the validated standard operating procedures (SOPs)[23], as defined and validated by the Eumorphia program (see: http://empress.har.mrc.ac.uk/). Briefly, we subjected our mice to non-invasive monitoring of body fat and lean mass by EchoMRI; energy expenditure analysis by indirect calorimetry (CLAMS system); intraperitoneal glucose tolerance test (ipGTT); insulin tolerance test (ipITT); blood sampling before and after a 24 fast; endurance exercise on a treadmill; non-invasive blood pressure measurement; and cold test. A summary of these methods is given in the supplementary materials and methods section. Animal experiments were approved by the ethic veterinary committee of the canton of Vaud - Switzerland (Permit IDs 2307 and 2307-1).

Quantitative RT-PCR. qRT-PCR was performed as already described[27,28]. Briefly, RNA was extracted from tissues using TRIzol reagent (Invitrogen). Complementary DNA was generated using QuantiTect Rev (Qiagen). The real-time PCR measurement of individual cDNAs was performed using SYBR green dye to measure duplex DNA formation with the LightCycler System (Roche Diagnostics). Primer sequences are listed in the supplementary materials and methods section.

Complex I, complex IV and citrate synthase activity assays. Complex I, complex IV and citrate synthase enzymatic activities were measured in homogenates of gastrocnemius muscle of $Sirt3^{skm+/+}$ and $Sirt3^{skm-/-}$ or of livers of $Sirt3^{hep+/+}$ and $Sirt3^{hep-/-}$ mice using the respective enzyme activity assay kits (Mitosciences), as reported elsewhere[29].

Mitochondrial isolation, immunoprecipitation and western blot analysis. Mitochondria were isolated from tissues following a previously described protocol[30]. Isolated mitochondria were lysed in RIPA lysis buffer containing protease inhibitors and supplemented with 5 mM NAM and 1 mM sodium butyrate. Immunoprecipitations were performed as described previously[28]. Protein extracts

were separated by SDS-PAGE. α-Sirt3 (home-made rabbit polyclonal against the peptides CDLMQRERGKLDGQDR and STPSGIPDFRSPGSGL), α-Total OxPhos (MitoSciences, MS604), α-Ndufa9 (Abcam, ab14713), α-AcK (Cell Signaling, 9441), α-Sod2 (Santa Cruz, sc-133254 for IP, sc-3008 for WB), and α-porin (Calbiochem, 529536) antibodies were used to detect the respective proteins.

Analysis of blood metabolites. For β-hydroxybutyrate (BHBA) analysis, plasma samples were precipitated with 1 M perchloric acid on ice. After centrifugation the supernatant was neutralized using 2M KOH, 0.5 M 2-(N-morpholino)ethanesulfonic acid (MES). BHBA concentrations were measured using LC-MS/MS in the neutralized supernatant after removal of $KClO_4$. Amino acids and acylcarnitines were analyzed in plasma according to established LC-MS/MS methods[31,32].

Evaluation of oxidative stress. Sod2 and catalase enzyme activity; HNE; and the GSH/GSSG ratio were measured in liver or gastrocnemius muscle homogenates using a Sod2 and catalase enzyme activity assays (Cayman Chemicals); the OxiSelect HNE-His Adduct ELISA Kit (Cell Biolabs Inc.); or the Bioxytech GSH/GSSG-412 kit (OxisResearch TM), respectively, following the manufacturer's protocols.

ATP measurements. ATP was measured in samples from liver or skeletal muscle using the ATP determination kit (Molecular Probes, Invitrogen), following previous reports[33] and the manufacturer's instructions. Briefly, tissues were weighed and lysed in 600 µl of 6% (v/v) perchloric acid, and centrifuged at 4000xg for 10 minutes at 4°C. 500 µl of the supernatant were neutralized with 200 µl of 2.5 M KOH, and precipitate was removed by centrifugation at 4000 xg for 5 minutes at 4°C. 10 µl of a 1:10 dilution of the samples in 0.1 M Tris-HCl – 2 mM EDTA buffer (TE) were placed in an appropriate bioluminescence plate, and luciferase activity was measured after addition of 100µl of the reaction solution, with a lag time of 1 second and an integration time of 3 seconds using a Glomax luminometer (Promega).

Preparation and culture of primary mouse hepatocytes and determination of oxygen consumption rates. Liver cells were prepared by the two-step collagenase method[34] from post-absorptive male mice (25–30 g) after anaesthesia with ketamin/xylazin (1 mg/100 g body weight). Cell viability (>80%) was checked by trypan blue exclusion. Primary culture of hepatocytes was seeded at 1.5×10^4 per well on rat-ail collagen type 1 (BDpharmingen) either on coated XF-96 cell culture plates (Seahorse) or on 12-well plates in serum-free DMEM (4.5 g/l glucose) medium. Four hours after seeding, the medium was replaced by a glucose and serum free DMEM medium, supplemented with lactate 10 mM and pyruvate 1 mM and the cells were infected with either an adenovirus containing a GFP construct (Adeno-GFP) or an adenovirus containing a recombinase Cre (Adeno-Cre) construct at a multiplicity of infection (MOI) of 15. Cellular oxygen consumption rate (OCR) was measured by Seahorse XF96 forty-eight hours after infection of cells as previously reported[35].

Statistical analyses. Statistical analyses were performed with non-parametric Student's *t*-test. Data are expressed as mean ± SEM and p values smaller than 0.05 were considered as statistically significant. Statistical significance is displayed as * ($p < 0.05$) or ** ($p < 0.01$).

1. Schwer, B., North, B. J., Frye, R. A., Ott, M. & Verdin, E. The human silent information regulator (Sir)2 homologue hSIRT3 is a mitochondrial nicotinamide adenine dinucleotide-dependent deacetylase. *J Cell Biol* **158**, 647–657 (2002).
2. Lombard, D. B. *et al.* Mammalian Sir2 homolog SIRT3 regulates global mitochondrial lysine acetylation. *Mol Cell Biol* **27**, 8807–8814 (2007).
3. Shi, T., Wang, F., Stieren, E. & Tong, Q. SIRT3, a mitochondrial sirtuin deacetylase, regulates mitochondrial function and thermogenesis in brown adipocytes. *J Biol Chem* **280**, 13560–13567 (2005).
4. Hokari, F. *et al.* Muscle contractile activity regulates Sirt3 protein expression in rat skeletal muscles. *J Appl Physiol* **109**, 332–340 (2010).
5. Palacios, O. M. *et al.* Diet and exercise signals regulate SIRT3 and activate AMPK and PGC-1alpha in skeletal muscle. *Aging (Albany NY)* **1**, 771–783 (2009).
6. Hirschey, M. D. *et al.* SIRT3 regulates mitochondrial fatty-acid oxidation by reversible enzyme deacetylation. *Nature* **464**, 121–125 (2010).
7. Jing, E. *et al.* Sirtuin-3 (Sirt3) regulates skeletal muscle metabolism and insulin signaling via altered mitochondrial oxidation and reactive oxygen species production. *Proceedings of the National Academy of Sciences of the United States of America* **108**, 14608–14613 (2011).
8. Kim, H. S. *et al.* SIRT3 is a mitochondria-localized tumor suppressor required for maintenance of mitochondrial integrity and metabolism during stress. *Cancer Cell* **17**, 41–52 (2010).
9. Qiu, X., Brown, K., Hirschey, M. D., Verdin, E. & Chen, D. Calorie restriction reduces oxidative stress by SIRT3-mediated SOD2 activation. *Cell Metab* **12**, 662–667 (2010).
10. Someya, S. *et al.* Sirt3 mediates reduction of oxidative damage and prevention of age-related hearing loss under caloric restriction. *Cell* **143**, 802–812 (2010).
11. Sundaresan, N. R. *et al.* Sirt3 blocks the cardiac hypertrophic response by augmenting Foxo3a-dependent antioxidant defense mechanisms in mice. *J Clin Invest* **119**, 2758–2771 (2009).
12. Tao, R. *et al.* Sirt3-mediated deacetylation of evolutionarily conserved lysine 122 regulates MnSOD activity in response to stress. *Mol Cell* **40**, 893–904 (2010).
13. Ahn, B. H. *et al.* A role for the mitochondrial deacetylase Sirt3 in regulating energy homeostasis. *Proc Natl Acad Sci U S A* **105**, 14447–14452 (2008).
14. Hirschey, M. D. *et al.* SIRT3 Deficiency and Mitochondrial Protein Hyperacetylation Accelerate the Development of the Metabolic Syndrome. *Mol Cell* (2011).
15. Hallows, W. C. *et al.* Sirt3 promotes the urea cycle and fatty acid oxidation during dietary restriction. *Mol Cell* **41**, 139–149 (2011).
16. Kong, X. *et al.* Sirtuin 3, a new target of PGC-1alpha, plays an important role in the suppression of ROS and mitochondrial biogenesis. *PLoS One* **5**, e11707 (2010).
17. Miniou, P. *et al.* Gene targeting restricted to mouse striated muscle lineage. *Nucleic Acids Res* **27**, e27 (1999).
18. Postic, C. *et al.* Dual roles for glucokinase in glucose homeostasis as determined by liver and pancreatic beta cell-specific gene knock-outs using Cre recombinase. *The Journal of biological chemistry* **274**, 305–315 (1999).
19. Shimazu, T. *et al.* SIRT3 deacetylates mitochondrial 3-hydroxy-3-methylglutaryl CoA synthase 2 and regulates ketone body production. *Cell Metab* **12**, 654–661 (2010).
20. Seale, P. *et al.* Prdm16 determines the thermogenic program of subcutaneous white adipose tissue in mice. *The Journal of clinical investigation* **121**, 96–105 (2011).
21. Ortega-Molina, A. *et al.* Pten positively regulates brown adipose function, energy expenditure, and longevity. *Cell metabolism* **15**, 382–394 (2012).
22. Champy, M. F. *et al.* Mouse functional genomics requires standardization of mouse handling and housing conditions. *Mammalian genome : official journal of the International Mammalian Genome Society* **15**, 768–783 (2004).
23. Champy, M. F. *et al.* Genetic background determines metabolic phenotypes in the mouse. *Mamm Genome* **19**, 318–331 (2008).
24. Donovan, M. J., Paulino, G. & Raybould, H. E. Activation of hindbrain neurons in response to gastrointestinal lipid is attenuated by high fat, high energy diets in mice prone to diet-induced obesity. *Brain Res* **1248**, 136–140 (2009).
25. West, D. B., Boozer, C. N., Moody, D. L. & Atkinson, R. L. Dietary obesity in nine inbred mouse strains. *Am J Physiol* **262**, R1025–1032 (1992).
26. Argmann, C. A., Chambon, P. & Auwerx, J. Mouse phenogenomics: the fast track to "systems metabolism". *Cell metabolism* **2**, 349–360 (2005).
27. Yamamoto, H. *et al.* NCoR1 is a conserved physiological modulator of muscle mass and oxidative function. *Cell* **147**, 827–839 (2011).
28. Canto, C. *et al.* AMPK regulates energy expenditure by modulating NAD+ metabolism and SIRT1 activity. *Nature* **458**, 1056–1060 (2009).
29. Houtkooper, R. H. *et al.* The metabolic footprint of aging in mice. *Sci Rep* **1**, 134 (2011).
30. Frezza, C., Cipolat, S. & Scorrano, L. Organelle isolation: functional mitochondria from mouse liver, muscle and cultured fibroblasts. *Nat Protoc* **2**, 287–295 (2007).
31. Koutnikova, H. *et al.* Identification of the UBP1 locus as a critical blood pressure determinant using a combination of mouse and human genetics. *PLoS Genet* **5**, e1000591 (2009).
32. Piraud, M. *et al.* ESI-MS/MS analysis of underivatised amino acids: a new tool for the diagnosis of inherited disorders of amino acid metabolism. Fragmentation study of 79 molecules of biological interest in positive and negative ionisation mode. *Rapid Commun Mass Spectrom* **17**, 1297–1311 (2003).
33. Khan, H. A. Bioluminometric assay of ATP in mouse brain: Determinant factors for enhanced test sensitivity. *J Biosci* **28**, 379–382 (2003).
34. Berry, M. N. & Friend, D. S. High-yield preparation of isolated rat liver parenchymal cells: a biochemical and fine structural study. *The Journal of cell biology* **43**, 506–520 (1969).
35. Watanabe, M. *et al.* Bile acids induce energy expenditure by promoting intracellular thyroid hormone activation. *Nature* **439**, 484–489 (2006).

Acknowledgements

This study was supported by grants of the Ecole Polytechnique Fédérale de Lausanne, the Swiss National Science Foundation (31003A-124713), and the European Research Council Ideas program (Sirtuins; ERC-2008-AdG23118). JA is the Nestle Chair in Energy Metabolism (NCEM). PJFM benefited from a FEBS fellowship. The authors thank all the members of the Auwerx lab for inspiring discussions, and Dr. Manuel Serrano (CNIO, Spain) for his help and support.

Author contributions

PJF-M and EJ (+) contributed equally to this work. PJF-M and EJ directed and performed all the experiments. CC participated in the immunoprecipitation experiments. PA participated in the mitochondrial complex activities assays. TH and NM performed the primary hepatocyte experiments. CC, EP and HY participated in the metabolic phenotyping of the mouse models. VB and SH performed the blood metabolite analysis. KS and JA directed all the work. PJF-M, CC, KS and JA wrote the manuscript. All authors reviewed the manuscript.

Additional information

Supplementary information accompanies this paper at http://www.nature.com/scientificreports

Competing financial interests: None of the authors have competing financial interests.

How to cite this article: Fernandez-Marcos, P.J. *et al.* Muscle or liver-specific Sirt3 deficiency induces hyperacetylation of mitochondrial proteins without affecting global metabolic homeostasis. *Sci. Rep.* **2**, 425; DOI:10.1038/srep00425 (2012).